

# Alternative evaluations of halos in nuclei

S. Karataglidis<sup>(a)</sup>, P. J. Dortmans<sup>(b)</sup>, K. Amos<sup>(b)</sup>, and C. Bennhold<sup>(c)</sup>

<sup>(a)</sup> *TRIUMF, 4004 Wesbrook Mall, Vancouver, British Columbia, V6T 2A3, Canada*

<sup>(b)</sup> *School of Physics, University of Melbourne, Parkville, Victoria, 3052, Australia*

<sup>(c)</sup> *Center of Nuclear Studies, Department of Physics, The George Washington University,  
Washington, D.C., 20052*

(September 25, 2018)

## Abstract

Data for the scattering of  ${}^6\text{He}$ ,  ${}^8\text{He}$ ,  ${}^9\text{Li}$ , and  ${}^{11}\text{Li}$  from hydrogen are analyzed within a fully microscopic folding model of proton-nucleus scattering. Current data suggest that of these only  ${}^{11}\text{Li}$  has a noticeable halo. The available data for the  ${}^6\text{Li}(\gamma, \pi^+){}^6\text{He}_{gs}$  reaction support the conclusion that  ${}^6\text{He}$  does not.

Much information has been learned concerning the nature of halos in nuclei from studies of heavy ion break up reactions in which the momentum distributions of the valence nucleons have been found to be very narrow [1]. This observation suggests matter distributions which extend well beyond the radius of the nuclear potential. Examples of halos found by this method are  $^{11}\text{Li}$  and  $^{11}\text{Be}$ , which are the most-studied of the neutron halos. Different neutron distributions in exotic nuclei, such as skins ( $^8\text{He}$ , for example), also have been studied using this method. While this approach has proved successful, it has the disadvantage of missing part of the initial state wave function of the halo nucleons [2]. Also, the breakup of  $^6\text{He}$  has been demonstrated to be a two-step process [3], in which the  $^5\text{He}$  fragment survives for a considerable amount of time as an  $\alpha - n$  resonance before it breaks up. This suggests that the effects of final state interactions are significant in this reaction, and so information concerning the initial state is lost. Nevertheless, the momentum of the valence neutron after the breakup is related to that of the  $^5\text{He}$  fragment by conservation of momentum, and the transverse component of the  $^5\text{He}$  momentum has been measured to be  $61.6 \pm 0.2 \text{ MeV}/c$  [3].

In order to study the initial state wave functions of the valence (halo) nucleons we look to alternatives in which the initial states are largely preserved in the reaction. Experiments have been performed for the scattering of heavy ions from hydrogen (see, for example, [4]). In the inverse kinematics this corresponds to proton scattering from the heavy ion, which directly measures the matter distribution of that ion. In particular, depending on the momentum transfer, such scattering may measure the density near the surface of the nucleus so that detailed information on the halo may be collected. Furthermore, it has been suggested [5] that charged pion photoproduction from nuclei may serve as a useful complementary probe of halo structures, especially as that reaction, like proton scattering, is also sensitive to the entire halo wave function. We have used both of these reactions to study the neutron distributions of  $^6\text{He}$ ,  $^8\text{He}$ ,  $^9\text{Li}$ , and  $^{11}\text{Li}$  in order to determine whether any of these nuclei has a neutron halo or skin.

It is now possible to predict observables from elastic proton–nucleus ( $pA$ ) scattering at intermediate energies (60 to 800 MeV) [6–8] using fully microscopic optical potentials that are specified by folding the appropriate effective nucleon–nucleon ( $NN$ ) interaction with the density as specified by a nucleon-based description of the nucleus. The description of the nucleus, in the form of one-body density matrix elements (OBDME), are determined from large space structure calculations which adequately describe the ground state properties and low excitation spectra, if pertinent. Once the effective interaction and OBDME are specified, the single particle (bound state) wave functions are required in order to calculate the scattering observables. For stable nuclei, these wave functions are assessed by their use in the analysis of electron scattering; for exotic nuclei, one may use wave functions obtained from analyses of scattering data for stable nuclei of equivalent or similar mass with reasonable success [9].

A realistic microscopic model of  $pA$  scattering is one that is based upon  $NN$   $g$  matrices, which are solutions of the Brueckner–Bethe–Goldstone ( $BBG$ ) equations. These equations are the generalization of the Lippmann–Schwinger equations when one admits nuclear medium modification effects of Pauli blocking and average background fields [10]. The  $g$  matrices converge to the  $t$  matrices as the density approaches zero. The on-shell values are consistent with measured  $NN$  scattering data at the incident energies of interest, and Ref. [11] contain those we have used. As we use a coordinate space folding model for

the  $pA$  optical potential [12], these  $g$  matrices are mapped into an effective interaction in coordinate space [10].

Several groups report shell model calculations of  ${}^6,8\text{He}$  and  ${}^9,11\text{Li}$ . Navrátil and Barrett [13] have made large-space shell model calculations using interactions obtained directly from the  $NN$   $g$  matrices, with the Reid93  $NN$  interaction as their base. Their calculations for  ${}^6\text{He}$  were done in a complete  $(0 + 2 + 4 + 6)\hbar\omega$  model space while those for  ${}^8\text{He}$ ,  ${}^9\text{Li}$  and  ${}^{11}\text{Li}$  were done in the smaller  $(0 + 2 + 4)\hbar\omega$  model space; the limitation arising from the dimensionality increasing with mass for a given space. Good results were found for the ground state properties in each case. For  ${}^6\text{He}$  specifically their calculations indicate that there is little or no need for this system to have a neutron halo to obtain agreement. For the other nuclei, they find spectra and ground state properties that are also quite good, although the calculated proton root-mean-square (rms) radii are small in comparison to the measured values. The cause of these discrepancies may be a halo-like distribution of the excess neutrons; the  $(0 + 2 + 4)\hbar\omega$  model space is not large enough to admit such halo characteristics for these nuclei [13]. These calculations may be contrasted with the results of our recent study [9] in which results of  $(0 + 2)\hbar\omega$  shell model calculations of  ${}^9\text{Li}$  and  ${}^{11}\text{Li}$ , made using phenomenological interactions, were reported. When using the wave functions obtained in those smaller space calculations, the available elastic proton scattering data at 60 and 68 MeV were well described.

We first consider elastic scattering of the heavy ions from hydrogen, data for which are available at 72A MeV for  ${}^6,8\text{He}$  and 62A MeV for  ${}^9,11\text{Li}$ . The calculations for the scattering from  ${}^9\text{Li}$  and  ${}^{11}\text{Li}$  are those presented in Ref. [9], while those for  ${}^6\text{He}$  and  ${}^8\text{He}$  used the OBDME as we have obtained from a complete  $(0 + 2 + 4)\hbar\omega$  model space calculation of those systems using the  $G$  matrix interaction of Zheng *et al.* [14]. The code OXBASH [15] was used for all calculations. We designate those calculations that use single-particle wave functions from the shell model calculations as “non-halo”. We estimate the effects of the halo by varying the single particle wave functions. In all cases, Woods-Saxon (WS) wave functions were used. Those which gave good reproduction of the elastic electron scattering form factors of  ${}^6\text{Li}$  [8] were used for the  ${}^6,8\text{He}$  calculations while those which reproduced the elastic electron scattering form factors of  ${}^9\text{Be}$  [7] were used in the calculations for  ${}^9\text{Li}$  and  ${}^{11}\text{Li}$ . In our analyses,  ${}^8\text{He}$  and  ${}^9\text{Li}$  act as controls;  ${}^8\text{He}$  is an example of a neutron skin and  ${}^9\text{Li}$  is a simple core nucleus. The single neutron separation energies for these nuclei are 2.137 MeV and 4.063 MeV for  ${}^8\text{He}$  [16] and  ${}^9\text{Li}$  [17], respectively. We may artificially ascribe a halo to these nuclei to ascertain if the procedure and data are sensitive enough to detect the flaw. To specify the “halo”, we adjusted the WS potentials such that the relevant neutron orbits are weakly bound. This guarantees an extensive neutron distribution. For  ${}^6\text{He}$ , the  $0p$ -shell binding energy was set to 2 MeV, which is close to the separation energy (1.87 MeV [16]) of a single neutron from  ${}^6\text{He}$ . For  ${}^9\text{Li}$  and  ${}^{11}\text{Li}$ , the halo was specified by setting the binding energy for the WS functions of the  $0p_{\frac{1}{2}}$  and higher orbits to 0.5 MeV [9].

The neutron density profiles for  ${}^6\text{He}$ ,  ${}^8\text{He}$ ,  ${}^9\text{Li}$ , and  ${}^{11}\text{Li}$  obtained from the present shell model calculations are shown in Fig. 1. Therein the dashed and solid lines portray, respectively, the profiles found with and without the halo conditions being implemented. The dot-dashed line in each case represents the proton density. As the folding process defines the optical potentials, the internal ( $r < r_{\text{rms}}$ ) region influences the predictions of differential cross sections, notably at large scattering angles. In this region the extensive (halo)

distribution exhibits a lower density, as the neutron strength is bled to higher radii. That effect characterized the proton halo in  $^{17}\text{F}^*$  as manifest in the  $^{17}\text{O}(\gamma, \pi^-)$  reaction [5]. The extended nature of the halo also influences the optical potentials as evidenced in changes to the cross sections at small momentum transfers (typically  $< 0.5 \text{ fm}^{-1}$  or  $\theta_{c.m.} < 15^\circ$  for beam energies between  $60A$  and  $70A$  MeV).

The predicted differential cross sections for the scattering of  $^{6,8}\text{He}$  and  $^{9,11}\text{Li}$  from hydrogen are presented in Figs. 2 and 3. In Fig. 2 we display the results to  $80^\circ$  ( $q \sim 2.5 \text{ fm}^{-1}$ ) and compare them with the data taken by Korshennikov *et al.* [4,18] using  $70.5A$  MeV  $^6\text{He}$  and  $72A$  MeV  $^8\text{He}$  beams, and by Moon *et al.* [19] using  $60A$  MeV  $^9\text{Li}$  and  $62A$   $^{11}\text{Li}$  beams. The forward angle results specifically, for which there are no data, are shown in Fig. 3 to emphasize the influence on the predictions by the extension of the halo ( $r > r_{\text{rms}}$ ). In both figures the solid curves depict the non-halo results while the dashed curves are those with the halo.

As is evident in Fig. 2, the data for our two controls,  $^8\text{He}$  and  $^9\text{Li}$ , are sufficient to resolve the question of whether these nuclei exhibit halos. In both cases the data above  $50^\circ$  are reproduced by the non-halo results suggesting that these nuclei do not have extended neutron distributions. This gives confidence in our ability to use such data to determine if a nucleus has a halo. That is confirmed in the case of the scattering of  $^{11}\text{Li}$  from hydrogen as the data clearly support a halo structure. There are differences evident between the halo and the non-halo predictions with these nuclei when one considers small angle scattering, where the influence of the Coulomb interaction is quite important. We present the results of our calculations for small angle scattering in Fig. 3. For  $^9\text{Li}$ , the difference between the halo and non-halo results is small which supports the notion that this nucleus is a close-packed system. This is contrasted by the results for both  $^8\text{He}$  and  $^{11}\text{Li}$ : the difference between the halo and non-halo results for  $^{11}\text{Li}$  is greater, suggesting again the halo structure, but the difference is greatest in  $^8\text{He}$ . Together with the large angle scattering data this suggests the neutron skin structure for  $^8\text{He}$  serves to dilute the charge distribution stemming from the two protons while pushing the density of the neutrons uniformly to larger radii as is shown in Fig. 1.

We now turn our attention to  $^6\text{He}$ . As shown in Fig. 2, the existing  $^6\text{He}$  data range only to  $50^\circ$  ( $q \sim 1.6 \text{ fm}^{-1}$ ). This is insufficient to discriminate between the halo and non-halo structures. As confirmed by the data and optical model analysis of Korshennikov *et al.* [4], our results are almost identical to those from  $p$ - $^6\text{Li}$  scattering, but only in the region where the data were taken for the  $p$ - $^6\text{He}$  scattering. Beyond this region there is a sufficient difference between the calculations to determine if  $^6\text{He}$  exhibits a halo. Data are needed beyond  $50^\circ$  to make such an assessment. The small angle scattering shown in Fig. 3 is consistent with the result for  $^9\text{Li}$  in showing little difference between the halo and non-halo results.

We may also study  $^6\text{He}$  via the  $^6\text{Li}(\gamma, \pi^+)^6\text{He}_{gs}$  reaction. We have calculated the cross sections for this reaction at  $E_\gamma = 200$  MeV using the DWIA model of Tiator and Wright [20]. As the  $^6\text{He}$  ground state is the isobaric analogue of the  $0^+; 1$  (3.563 MeV) state in  $^6\text{Li}$ , we have used the OBDME for the transition to that state in  $^6\text{Li}$ , as obtained from a complete  $(0 + 2 + 4)\hbar\omega$  shell model calculation [8]. The non-halo result corresponds to a calculation using harmonic oscillator single-particle wave functions with  $\hbar\omega = 12.65$  MeV [8]. Those wave functions are also used for the initial  $^6\text{Li}$  state to obtain the halo result with

the final  ${}^6\text{He}$  state being specified by WS wave functions in the  $0p$ -shell and higher orbitals only as given in the halo calculation of the scattering presented above. Such a specification introduces a problem in normalization with the  $0p_{\frac{3}{2}}$  wave functions. The overlap of the HO and WS  $0p_{\frac{3}{2}}$  radial wave functions is 0.96, hence the wave functions preserve the norm to within 4%. Both results are compared to the data of Shaw *et al.* [21] (circles) and Shoda *et al.* [22] (squares) in Fig. 4, wherein the halo and non-halo calculations are displayed by the dashed and solid lines respectively. From the available data one may infer that the non-halo result is favored, but this is due to the datum at  $137^\circ$  only. Note that our non-halo result is similar to that found by Doyle *et al.* [23] in which they used a  $0\hbar\omega$  model of structure and no specific halo structure was specified. More data in the region of the possible minimum as well as at large angles are needed to confirm the conjecture that  ${}^6\text{He}$  does not have a halo structure.

In summary, the available scattering data from hydrogen confirm that  ${}^{11}\text{Li}$  is a halo nucleus, while the analysis of the scattering data correctly determines that both  ${}^8\text{He}$  and  ${}^9\text{Li}$  are not. The low-angle scattering results also suggest that  ${}^8\text{He}$  is a neutron skin nucleus, as found from breakup reactions. The available scattering data for  ${}^6\text{He}$  from hydrogen are not extensive enough to discriminate between the halo and non-halo scenarios; in the measured region they suggest for  ${}^6\text{He}$  a very similar matter distribution compared to  ${}^6\text{Li}$ . The complementary  ${}^6\text{Li}(\gamma, \pi^+){}^6\text{He}$  reaction data suggest the non-halo hypothesis although more data are required to confirm this result. The analysis presented here demonstrates the need to study halo nuclei with complementary probes and reaction channels.

Financial support from the Natural Sciences and Engineering Research Council of Canada, the Australian Research Council, and Department of Energy Grant no. DE-FG02-95ER-40907 is gratefully acknowledged.

## REFERENCES

- [1] P. G. Hansen, A. S. Jensen, and B. Jonson, *Ann. Rev. Nucl. Part. Sci.* **45**, 591 (1995).
- [2] P. G. Hansen, *Phys. Rev. Lett.* **77**, 1016 (1996); H. Esbensen, *Phys. Rev. C* **53**, 2007 (1996).
- [3] D. Aleksandrov, *et al.*, *Nucl. Phys.* **A633**, 234 (1998).
- [4] A. A. Korshennikov, *et al.*, *Nucl. Phys.* **A617**, 45 (1997).
- [5] S. Karataglidis and C. Bennhold, *Phys. Rev. Lett.* **80**, 1614 (1998).
- [6] S. Karataglidis, P. J. Dortmans, K. Amos, and R. de Swiniarski, *Phys. Rev. C* **52**, 861 (1995); P. J. Dortmans, K. Amos, S. Karataglidis, and J. Raynal, *Phys. Rev. C* **58**, 2249 (1998).
- [7] P. J. Dortmans, K. Amos, and S. Karataglidis, *J. Phys. G* **23**, 183 (1997)
- [8] S. Karataglidis, B. A. Brown, P. J. Dortmans, and K. Amos, *Phys. Rev. C* **55**, 2826 (1997).
- [9] S. Karataglidis, P. G. Hansen, B. A. Brown, K. Amos, and P. J. Dortmans, *Phys. Rev. Lett.* **79**, 1447 (1997).
- [10] P. J. Dortmans and K. Amos, *Phys. Rev. C* **49**, 1309 (1994).
- [11] M. Lacombe, B. Loiseau, J. M. Richard, R. Vinh Mau, J. Côté, P. Pirès, and R. de Tourreil, *Phys. Rev. C* **21**, 861 (1980); R. Machleidt, K. Hollinde, and Ch. Elster, *Phys. Re.* **149**, 1 (1987); L. Jäde and H. V. von Geramb, *Phys. Rev. C* **55**, 57 (1997).
- [12] J. Raynal, computer code DWBA91 (NEA1209/02).
- [13] P. Navrátil and B. R. Barrett, *Phys. Rev. C* **54**, 2986 (1996); *ibid* *C* **57**, 3119 (1998).
- [14] D. C. Zheng, B. R. Barrett, J. P. Vary, W. C. Haxton, and C.-L. Song, *Phys. Rev. C* **52**, 2488 (1995).
- [15] OXBASH-MSU (the Oxford-Buenos-Aries-Michigan State University shell model code). A. Etchegoyen, W. D. M. Rae, and N. S. Godwin (MSU version by B. A. Brown, 1986); B. A. Brown, A. Etchegoyen, and W. D. M. Rae, MSUCL Report Number 524 (1986) (unpublished).
- [16] F. Ajzenberg-Selove, *Nucl. Phys.* **A490**, 1 (1988).
- [17] F. Ajzenberg-Selove, *Nucl. Phys.* **A506**, 1 (1990).
- [18] A. A. Korshennikov, *et al.*, *Phys. Lett.* **316B**, 38 (1993).
- [19] C.-B. Moon, *et al.*, *Phys. Lett.* **297B**, 39 (1992).
- [20] L. Tiator and L.E. Wright, *Phys. Rev. C* **30**, 989 (1984).
- [21] J. Shaw, T. Kobayashi, W. Clayton, L. Ghedira, D. Myers, P. Stoler, P. K. Teng, E. J. Winhold, and J. H. J. Distelbrink, *Phys. Rev. C* **43**, 1800 (1991).
- [22] K. Shoda, O. Sasaki, and T. Kohmura, *Phys. Lett.* **101B**, 124 (1981).
- [23] B. C. Doyle, Nimai C. Mukhopadhyay, and R. S. Wittman, *Phys. Rev. C* **52**, 1957 (1995).

FIGURES

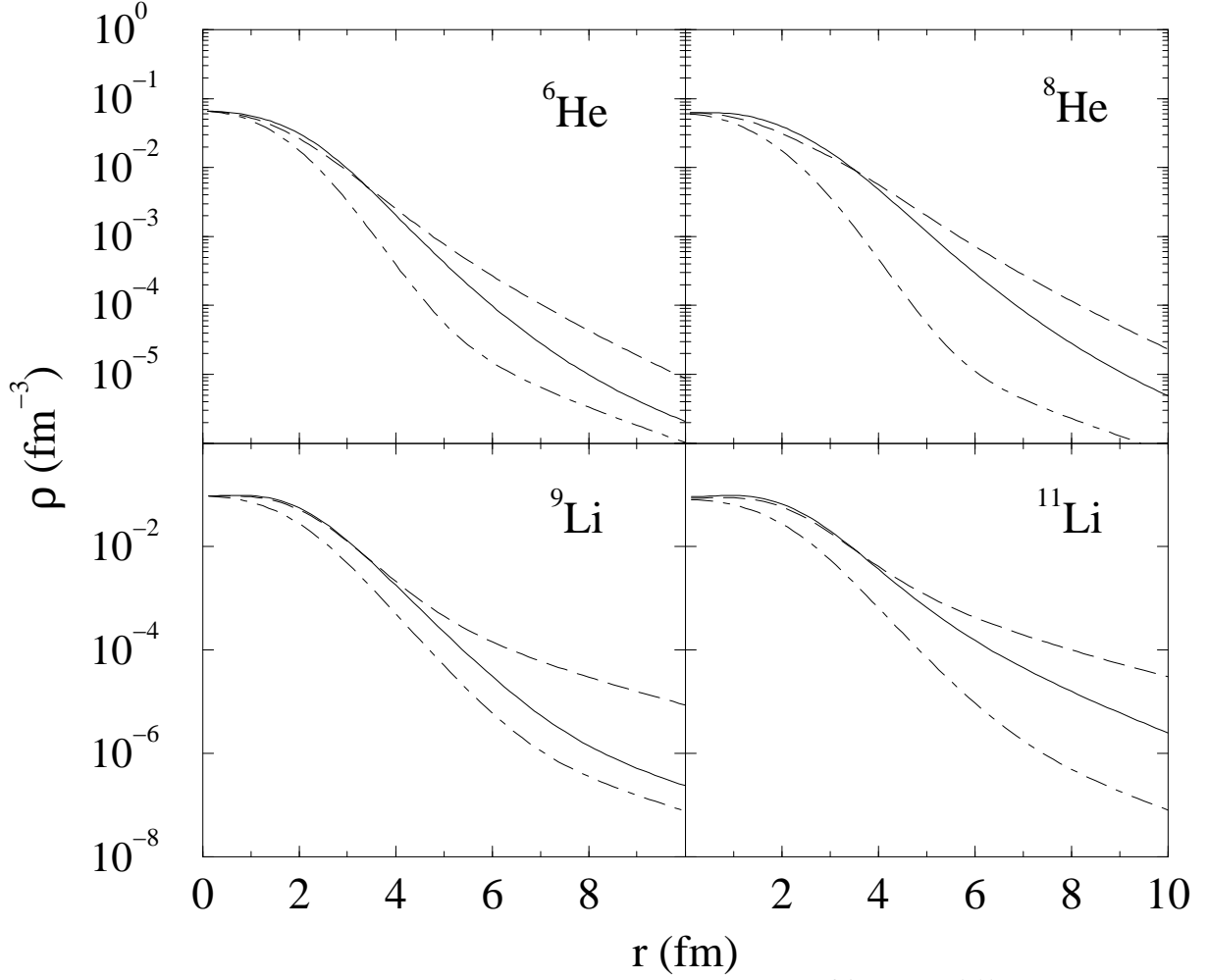


FIG. 1. The (shell model) neutron density profiles for the nuclei  ${}^{6,8}\text{He}$  and  ${}^{9,11}\text{Li}$ . The dashed and solid curves represent, respectively, the profiles when a halo is and is not contained in those structures. The dot-dashed lines represent the proton density for each nucleus.

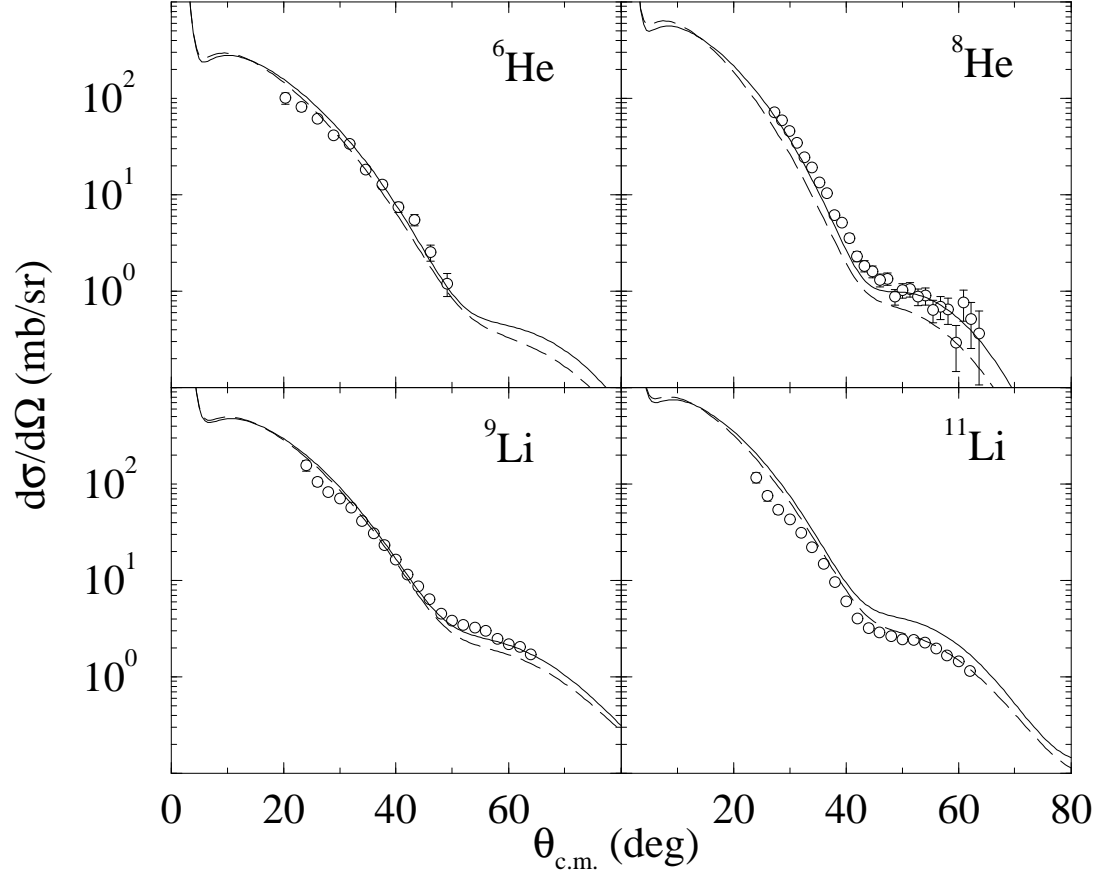


FIG. 2. Predictions of the differential cross sections from the scattering of 72A MeV  ${}^6,8\text{He}$  and of 62A MeV  ${}^9,11\text{Li}$  from hydrogen compared with experimental data. The data are from Refs. [18,4,19] and the results, assuming that each nucleus has (does not have) a halo structure, are portrayed by the dashed (solid) curves.



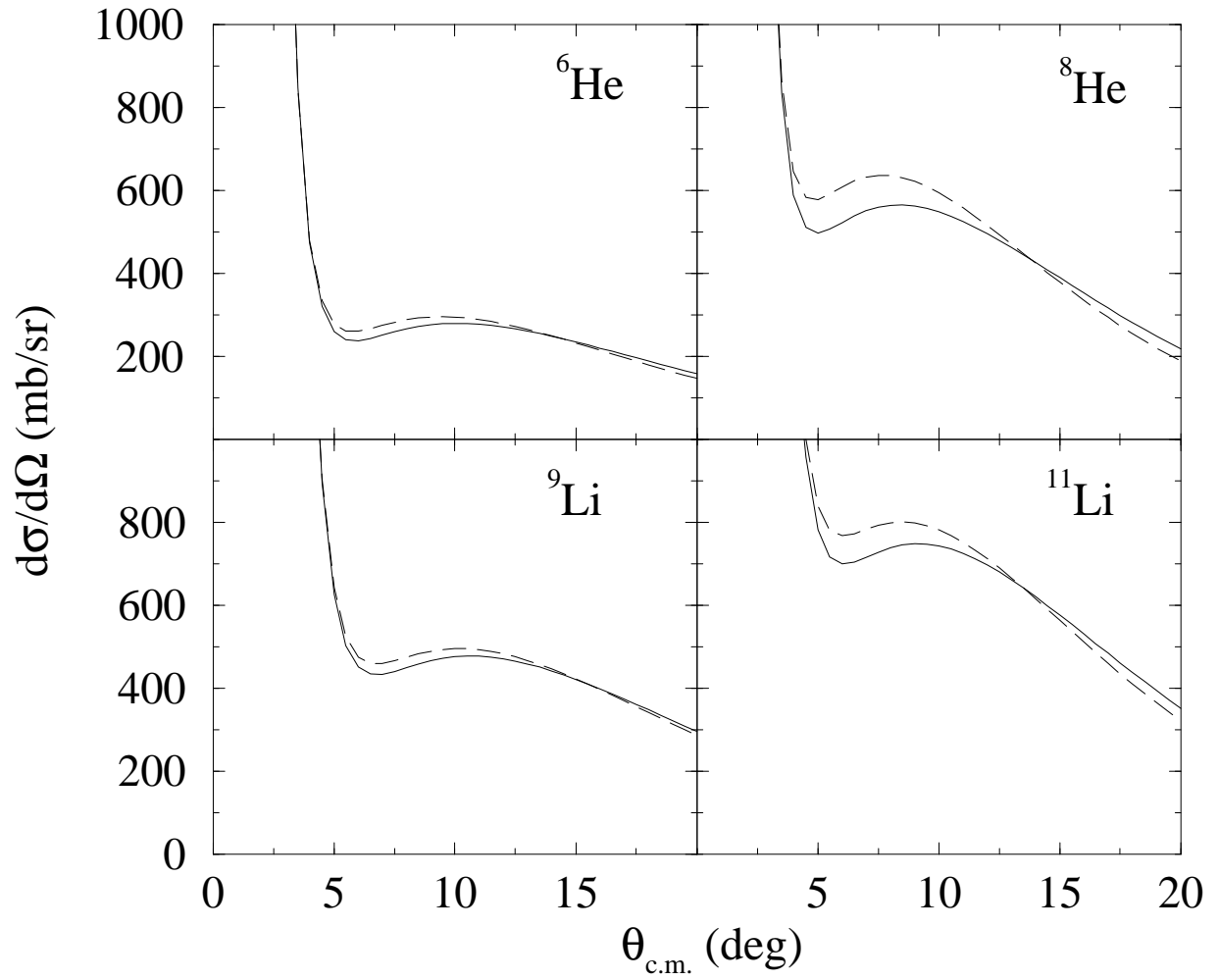


FIG. 3. Differential cross sections as shown in Fig. 2, but for small angles only.

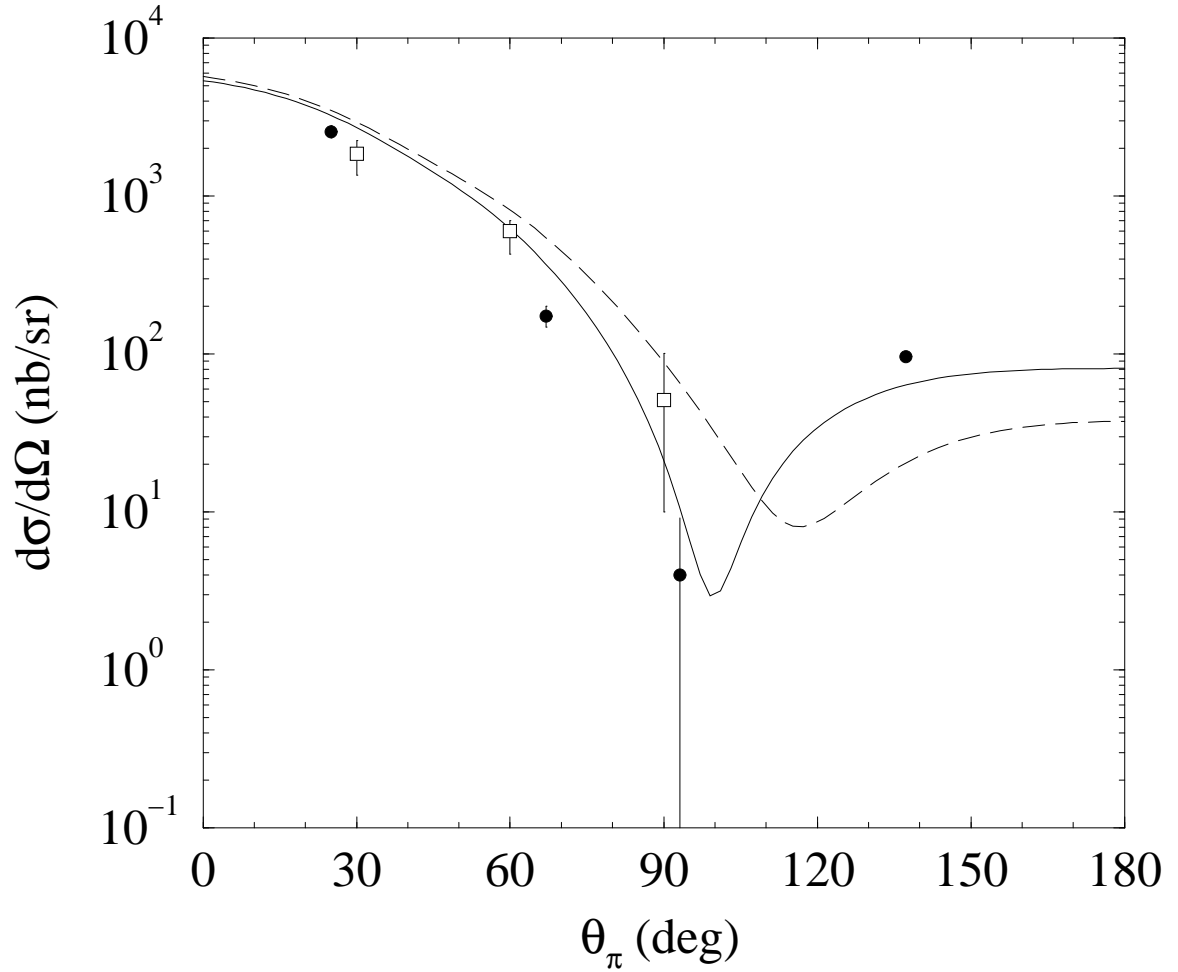


FIG. 4. The  ${}^6\text{Li}(\gamma, \pi^+){}^6\text{He}$  reaction for  $E_\gamma = 200$  MeV. The data of Shaw *et al.* (circles) [21] and Shoda *et al.* [22] (squares) are compared to the results with and without halo as displayed by the dashed and solid lines.